Investigating the influence of the jet from three nozzle and spear design configurations on Pelton runner performance by numerical simulation

S Petley[1], A Panagiotopoulos[1 2], D S Benzon[3], A Židonis[1], G A Aggidis[1], J S Anagnostopoulos[2], D E Papantonis[2]

[1] Lancaster University Renewable Energy Group and Fluid Machinery Group, Engineering Department, Lancaster University, Lancaster, LA1 4YR, UK
[2] School of Mechanical Engineering, National Technical University of Athens, Athens, Greece
[3] Mott MacDonald Ltd, Victory House, Trafalgar Place, Brighton, BN1 4FY, UK

Corresponding author: g.aggidis@lancaster.ac.uk (G A Aggidis)

Abstract. This paper reports the initial results of three dimensional CFD simulations of the jet – runner interactions in a twin jet horizontal axis Pelton turbine. More specifically, the analysis examines the impact of the nozzle and spear valve configuration on the performance of the runner. Previous research has identified that injectors with notably steeper nozzle and spear angles attain a higher efficiency than the industry standard. However, experimental testing of the entire Pelton system suggests that there appears to be an upper limit beyond which steeper angled designs are no longer optimal. In order to investigate the apparent difference between the numerical prediction of efficiency for the injector system and the obtained experimental results, four different jet configurations are analysed and compared. In the first configuration, the interaction between the runner and an ideal axisymmetric jet profile is investigated. In the final three configurations the runner has been coupled with the jet profile from the aforementioned injectors, namely the Standard design with nozzle and spear angles of 80° & 55° and two Novel designs with angles 110° & 70° and 150° & 90° respectively. The results are compared by examining the impact the jet shape has on the runner torque profile during the bucket cycle and the influence this has on turbine efficiency. All results provided incorporate the Reynolds-averaged Navier Stokes (RANS) Shear Stress Transport (SST) turbulence model and a two-phase Volume of Fluid (VOF) model, using the ANSYS® FLUENT® code. Therefore, this paper offers new insights into the optimal jet – runner interaction.

1. Introduction

The injector of a Pelton turbine is an important component as it converts the pressure energy available from the hydrostatic head to kinetic energy in the water jet, which is required to rotate the runner [1]. The injector is composed of two major components highlighted in Figure 1&2: a fixed nozzle and a spear that by actuation can move in and out of the nozzle to regulate the flowrate. Estimates of the pressure drop within the injector is usually of the order of 1% and losses arise primarily from surface friction with the walls of the injector resulting in a small reduction in velocity both around the perimeter

of the jet and at its core [2]. Moreover, the upstream bifurcation and branch pipe bend generates counter rotating Dean vortices in the flow and further interference is caused by the spear-rod support [3]. The secondary flows generated by these interactions lead to surface deformation, deviation and dispersion of the jet diameter [4]. Furthermore, due to the high Reynolds number, a turbulent interchange between the jet core and surface results in air entrainment and further surface deformation downstream, hence it is advantageous to minimise the distance between the nozzle and runner.

In recent decades numerical tools such as Computational Fluid Dynamics (CFD) have been applied to the development of Pelton turbines [5], however simulation of a full turbine is a demanding task due to the different fluid dynamics governing the flow in the separate parts, namely internal pipe flow and free surface flows. Therefore, the components are treated in isolation and the resulting high fidelity models offer a good prediction of the reasonable gains in efficiency from the optimisation of each component. CFD analysis has been used to test many factors governing the injector design: spear and nozzle diameter; spear and nozzle angle, spear rod support geometry and branchpipe design [6] .

Previous CFD studies of the injector have shown that steeper nozzle and spear angles, 110° and 70° respectively, attain a higher efficiency than the industry standard 80° and 55° by 0.4% for a 3D case study [7]. Further CFD study of the injectors indicated that even steeper angles 150° and 90° may further improve performance [8]. Subsequently, the three injector design configurations were tested in a Pelton model turbine at various speeds and flow rates to produce performance curves. These results indicated the steeper angled designs perform better than the standard design by some 1% at the best efficiency point for all tests, though the 110° and 70° performs slightly better than the 150° and 90° design, suggesting an upper limit beyond which steeper angled designs are no longer optimal. A summary of the experiment results is outlined in Section 2.

In order to investigate this apparent difference between the CFD and experimental results this paper analyses the influence of the nozzle and spear angle on the jet – runner interaction by considering four case studies. The first is an ideal jet, with uniform velocity profile and the following three will use the obtained velocity profiles from the three aforementioned injector designs. All simulations are carried out using the Reynolds-averaged Navier Stokes (RANS) k-ω Shear Stress Transport (SST) turbulence model and a two-phase Volume of Fluid (VOF) model within the ANSYS® FLUENT® code. The k-ω SST is the most widely applied turbulence model to the study of hydro impulse machines according to literature [5] and was selected after carrying out some preliminary assessments.

2. Experimental Results

Three injector designs were manufactured by Gilbert Gilkes & Gordon Ltd for experimental testing using the 75 kW Pelton test rig at the Laboratory for Hydraulic Machines, National Technical University of Athens (NTUA). The details of the injectors used in this study are shown in Figure 1 and Figure 2.

The testing was carried out in single jet operation using the upper jet for a range of speed and flow rates. The efficiency curves for the unit speed considered in this study, $n_{11} = 39$, are plotted against the non-dimensional flowrate, Q_{11k}, as shown in Figure 3. The efficiencies are normalised against the best efficiency test point. The characteristic equations of turbine unit speed, n_{11}, and unit flow, Q_{11k}, used to define the operation and performance of the turbine, are given in (1) – (5) below.

$$n_{11} = \frac{n \times D}{\sqrt{H}} \tag{1}$$

$$Q_{11k} = \frac{Q/N_j}{B^2 \times \sqrt{H}} \tag{2}$$

$$P_{out} = M\omega \tag{3}$$

$$P_{in} = \rho g H Q \tag{4}$$

$$\eta = \frac{P_{out}}{P_{in}} \tag{5}$$

Where n is the rotational speed of the runner, H is the net head, Q is the flow rate, N_j is the number of jets, M is the torque measured on the turbine shaft, ρ is the density of water and g is the acceleration due to gravity.

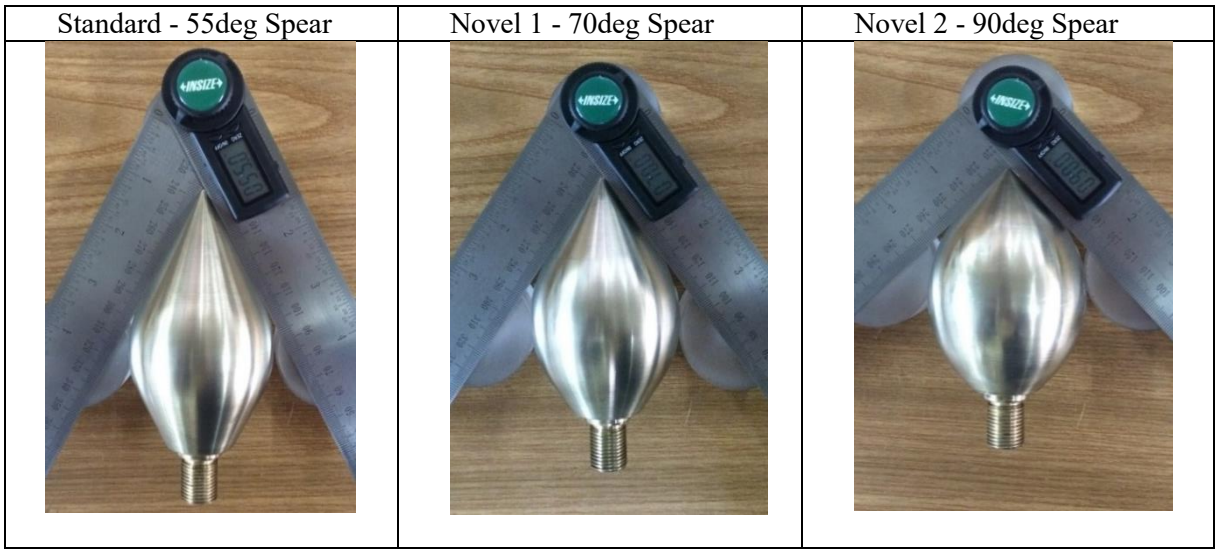

Figure 1. Pelton spears used for experimental tests.

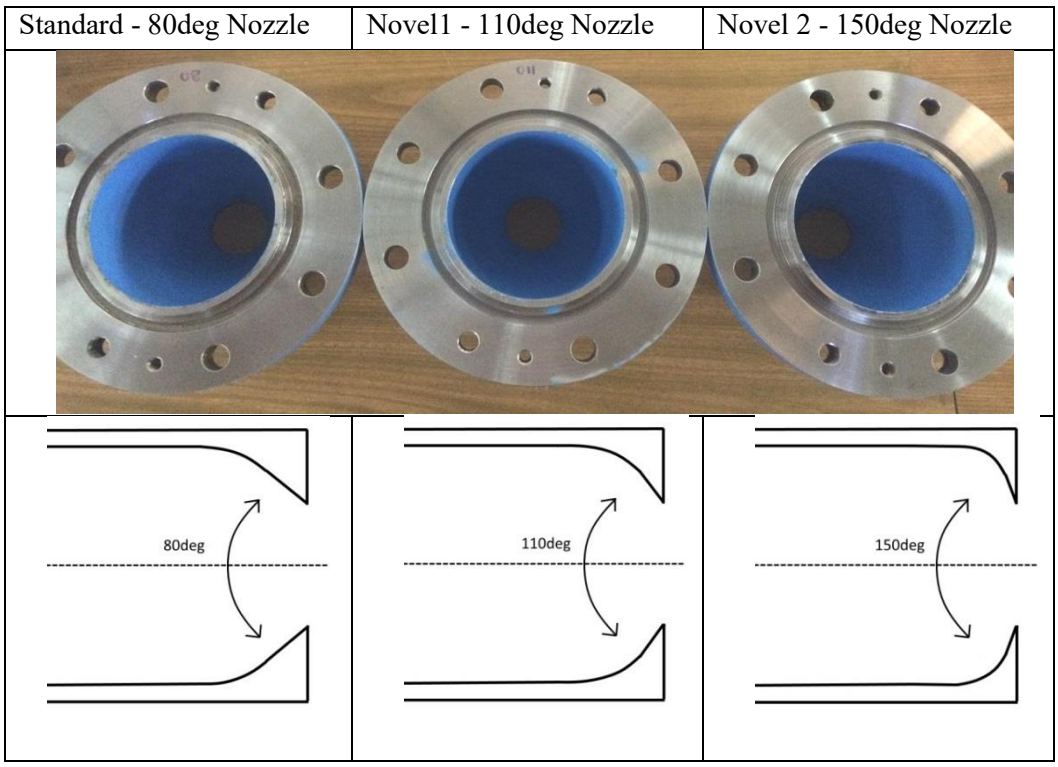

Figure 2. Pelton nozzles used for experimental testing.

The results indicate that the steeper angled designs (Novel 1 and Novel 2) perform much better than the Standard design, with the differences being more pronounced at lower flow rates where the losses through the injectors are greater. The efficiencies are normalised against the best efficiency test point. The gained efficiency increase is around 1% at the BEP for both Novel designs, however the Novel 1 design performs slightly better (around 0.8% higher normalised efficiency at lower flow rates to 0.2% at higher flow rates, at the nominal speed $n_{11} = 39$). Hence, the Novel 1 design achieves the highest increase in normalised efficiency compared to the Standard design, with a 1.2% increase at the BEP flow $Q_{11k} = 0.234$.

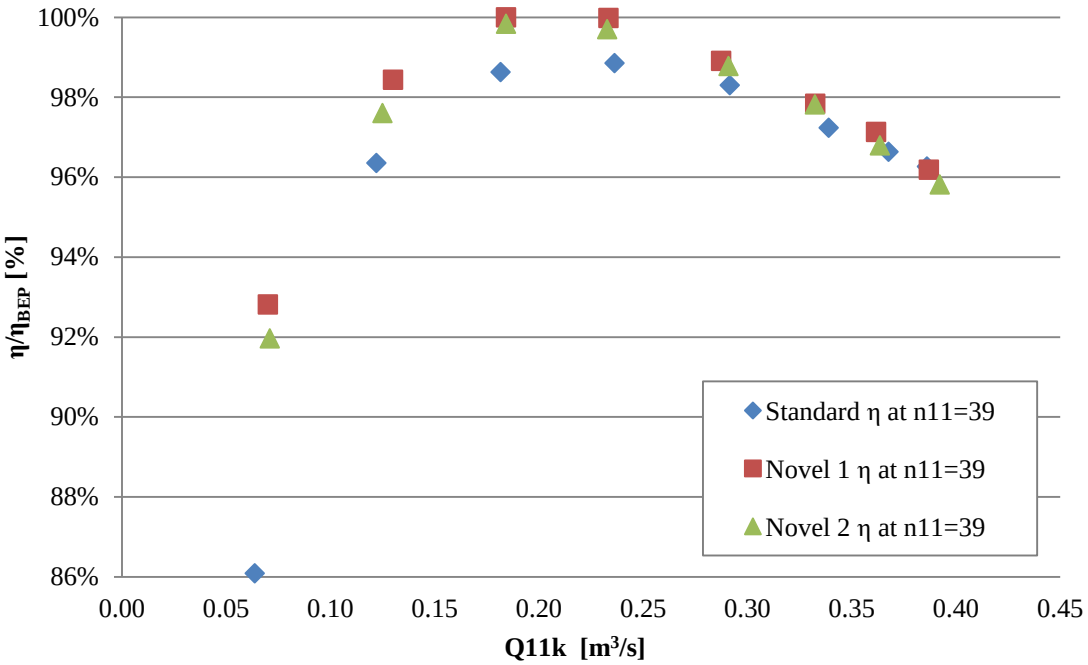

Figure 3. Pelton efficiency curves for 80/55, 110/70 and 150/90 injectors at n_{11}=39.

3. Numerical Model

3.1. Model Definition

As mentioned previously all simulations were carried out in FLUENT using the k-ω SST turbulence model and the VOF multiphase model at n_{11}=39 and the best efficiency flow rate. Because of the complexity of the analysis, a preliminary in-depth study was carried out to evaluate the influence of the main numerical parameters on the stability of the simulation, in line with [9]. In order to simplify the model and speed up convergence the numerical analysis can be broken down into two sub-simulations, the first highlighted in Figure 4, consists of a single injector for each of the three nozzle and spear combinations. The geometry of interest includes the nozzle, spear, spear rod, three spear holding vanes and the 60° pipe bend. The second sub-simulation, highlighted in Figure 5 consists of two domains, the stationary inlet and rotating runner, where only two (out of the full 18) buckets have been modelled. The two green circular planes in Figure 4 and Figure 5 represent 2 jet diameters distance from the nozzle opening and are the point at which the velocity profile representing the real jet is exported from the injector simulation and imported into the runner simulation in addition to the location at which the ideal jet boundary condition is defined.

The flow in the injector was modelled in steady state and following a mesh independence study a mesh of 9 million cells was used. Using the Coupled Solver the solution was run until the residuals had reached 10^{-6}. The mesh consisted of a combination of hexahedral cells in the straight sections of pipe

and in the areas surrounding the spear and jet after it has exited the nozzle, tetrahedral cells were used in the area surrounding the guide vanes and in the curved section of pipe. Mesh refinement was placed in the central core of the jet and in the area of the free surface using the Fluent adapt to volume fraction refinement tool.

The runner analysis is a transient simulation and the rotation is modelled using a sliding mesh approach, with an interface defined between the stationary jet and runner domains. The meshes consist of swept hexahedral cells within the stationary jet and a fully tetrahedral cells within the runner domain. Face sizing was used to match the element size across the interface in order to minimise numerical diffusion. Following a mesh independence study a mesh of 14 million cells was used and a conservative time step of 3.5219e-5 s, which equates to 0.2 degree rotation was chosen.

In all meshes inflation layers were applied to the wall boundaries and the minimum wall distance was calculated in order to keep the y+ value within the allowable limits of wall functions. The total pressure was set at the injector inlet according to the experimental test head. Velocity inlets were applied at the inlet of the runner mesh, with component values and the water volume fraction according to the imported profile for the real jet simulation. Pressure outlets were used at the interfaces and openings with relative static pressure of 0 Pa.

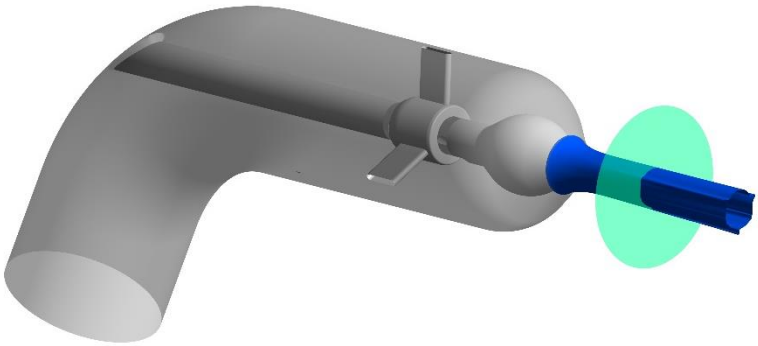

Figure 4. 3D injector simulation showing the plane used in the analysis.

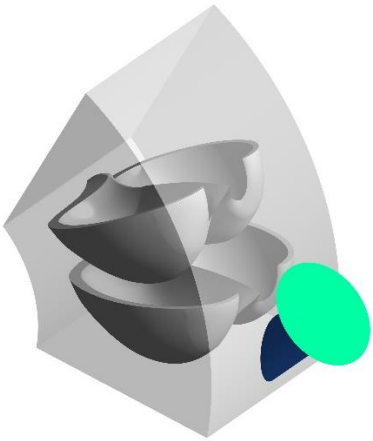

Figure 5. 3D runner simulation showing the corresponding plane used in the analysis.

3.2. Injector Flow Analysis

The losses through the injector can be calculated using the following equation (6).

$$P = \int_A \left(p + \frac{\rho u^2}{2}\right) \cdot u \, dA = \sum_1^n \left(p_i + \frac{\rho {u_i}^2}{2}\right) \cdot u_i \cdot A_i \tag{6}$$

Where P is the fluid power, p_i is static pressure, ρ_i is density of fluid, u_i is velocity of fluid at each individual mesh cell, i, A is the area at the cross-section and n is the number of the cells at the cross-section. Equation (6) defines the amount of power at any reference cross-section plane. Therefore, the accumulated losses in the region between the inlet plane and the reference outlet plane can be calculated using equation (7)

$$L_{ref} = \left(1 - \frac{P_{out}}{P_{in}}\right) \cdot 100\% \tag{7}$$

Where L_{ref} is the losses in the reference region, P_{in} is the power at the inlet reference plane and P_{out} is the power at the outlet reference plane.

The injector losses plotted at different jet diameters from the nozzle opening are shown in Figure 6, indicating that Novel 2 design is 0.4% more efficient than the Novel 1, which is more efficient than the Standard design by some 0.1%.

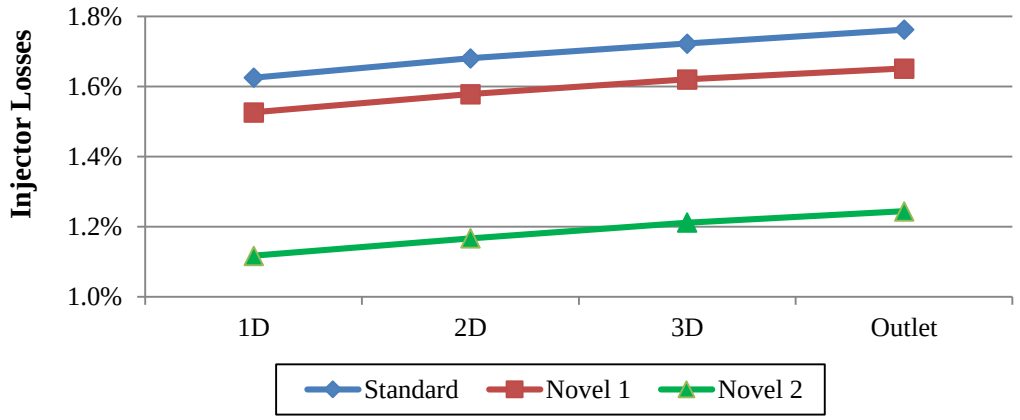

Figure 6. 3D Injector losses at different planes through the jet axis.

It is known from previous research [7] that the pipework bend induces counter rotating Dean vortices in the jet, which in themselves cause a bead to develop at the bottom of the jet corresponding to the inner pipework bend. Therefore, to determine the impact these secondary velocities has on the jet velocity, the profile through the vertical axis for the ideal case and three real cases in Figure 7. Other than some minor reduction in the velocity at the corners the jet is more uniform in the centre for the Novel designs, however the development of a bead at the bottom of the jet is revealed by the widening of the jet position, shown on the right hand side of Figure 7, which is more pronounced for the Novel cases. .

Chongji et al [10] demonstrated that with a larger spear stroke (i.e. higher flow rate) the jet vena contracta occurs much closer to the opening and the jet disperses much more severely particularly due to the bead formation on the side of the inner curvature of the bend. Moreover, as the spear stroke increased, the needle wall posed less of a frictional effect on the axial velocity at the same position. Therefore one can conclude that for the former corollary a more severe contraction angle, as is the case with the Standard design, results in a smaller bead formation and for the latter that a more uniform axial velocity through the jet, in the case of Novel 2, resulted in the hydraulic efficiency of the injector in isolation being the highest, despite the jet dispersion.

In order to investigate this apparent difference between injector losses and experimental efficiencies of the whole system the jet profiles were imported to the runner mesh, detailed in 3.3.

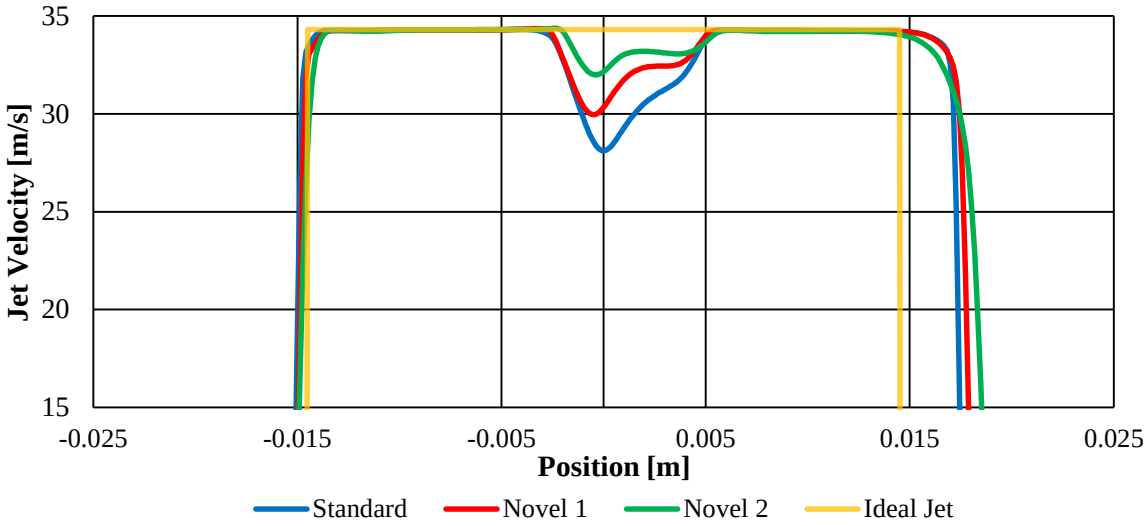

Figure 7. Jet Velocity Distribution at 2D from nozzle opening.

3.3. Ideal and Real Jet Comparison on Runner Performance

In FLUENT a moment monitor is defined to measure the torque, which writes out the final value of the moment for each timestep, this is defined for both the inside and outside surfaces (wall zones) of each bucket, highlighted for a representative bucket in Figure 8. The torque on the inside and outside of the buckets for the four case studies are plotted in Figure 9.

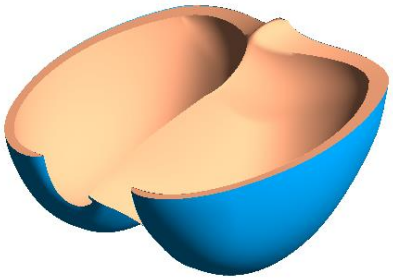

Figure 8. Moment monitor wall zone definition – inside (orange) and outside (blue).

Although all four configurations are characterised by a periodic trend the maximum torque obtained on the inside of the bucket differ slightly with all three designs being lower than the ideal-jet case, but Novel 1 being slightly higher than Novel 2 and Standard designs respectively.

The work done by a single bucket is calculated through numerically integrating the torque curve using the trapezium rule to give the area under the total torque curve, multiplying this by the number of buckets gives the work done by the runner. The efficiency can then be obtained by dividing the work done by the hydraulic input power derived from the boundary conditions specification. Table 1 compares the numerically obtained efficiency with the experimental results, which has been normalised against the efficiency of the ideal jet case, this is shown graphically in Figure 10. In the whole bucket cycle, the Novel 1 case was characterised by a greater energy exchange than the other real jet scenarios as reflected in the normalised efficiencies.

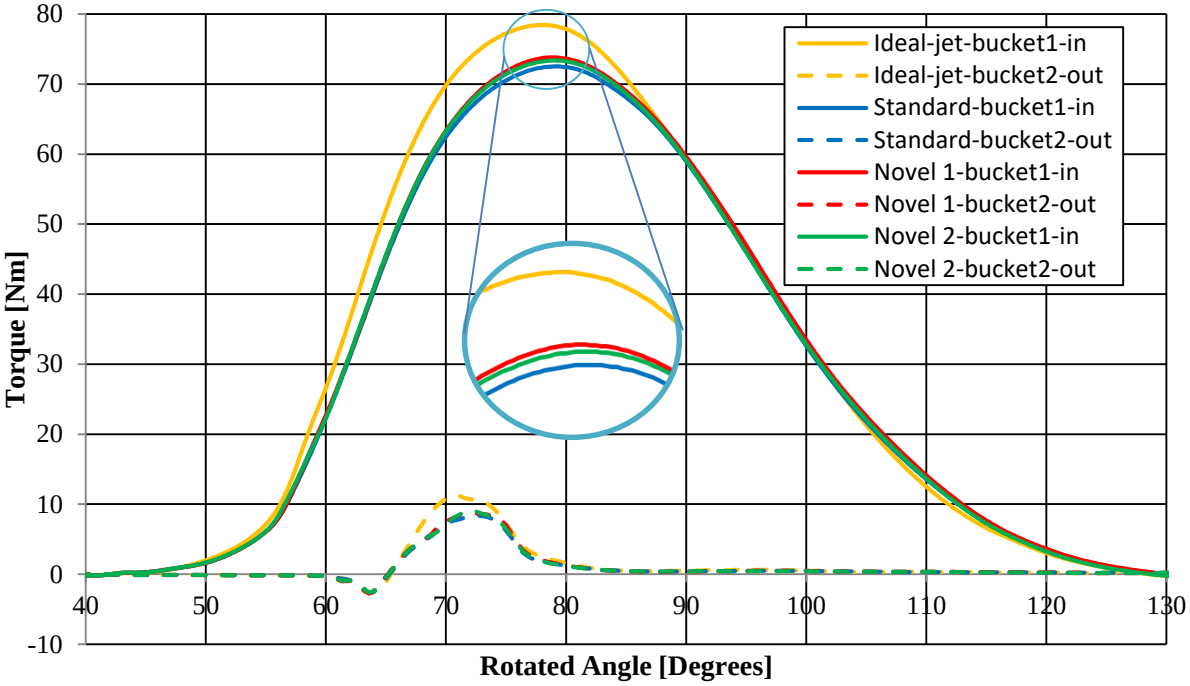

Figure 9. Torque curves on the inside and outside of the bucket for 4 configurations.

	Ideal Jet	Standard	Novel 1	Novel 2
Normalised CFD efficiency	**100%**	**98.3%**	**99.8%**	**99.7%**
Normalised experimental efficiency	**N/A**	**96.9%**	**98.3%**	**98.1%**

Table 1. Normalised efficiencies for the 4 case studies.

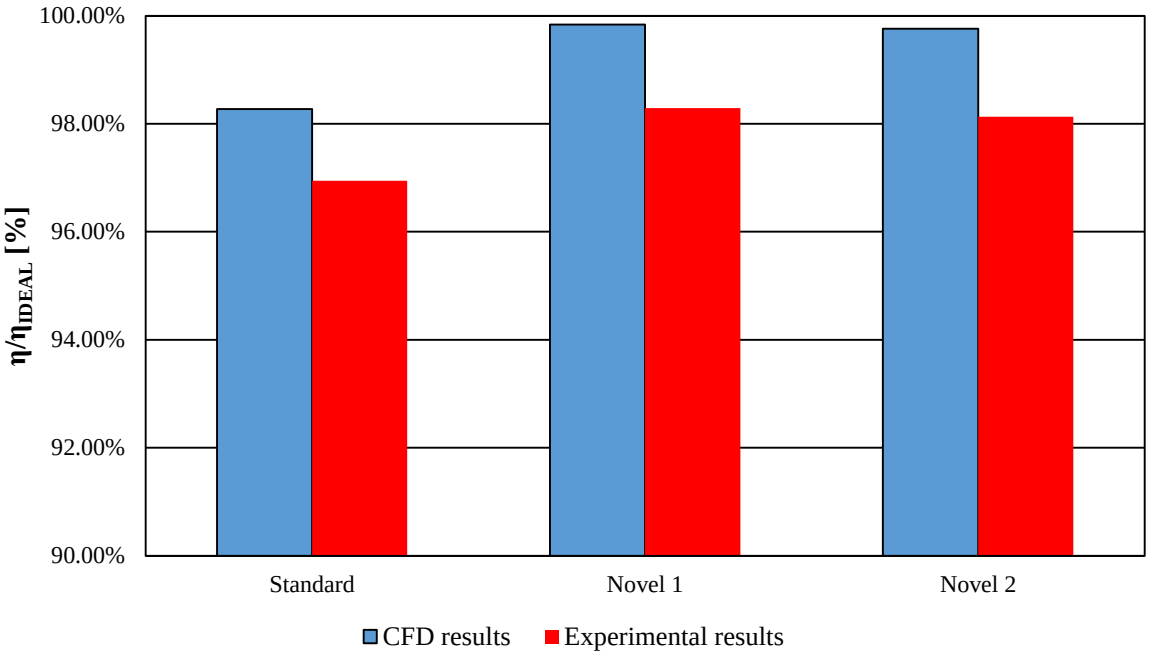

Figure 10. Comparison of the CFD and experimentally obtained efficiency for the 3 real cases normalised to the ideal CFD case.

It should be noted that the slight negative torque on the outside of the bucket (60° - 65° for bucket 2) is due to the negative pressure that is pulling the bucket, which arises during the jet cutting process as a result of the Coanda effect. This has been documented experimentally in [11] and [12].

As it can be seen in Table 1, reporting the comparison between numerical and experimental data, the error in the calculation of the is around 1.5% for each case study, this is slightly lower than the error orders of other numerical analyses carried out on Pelton turbines [9], however typically the CFD will over predict efficiency. Further impact of the shape of the jet and the influence on performance can be investigated by inspecting the free surface isosurface plots at 80^0 degrees rotation, as highlighted in Figure 11, from top left clockwise – ideal jet, Standard jet, Novel 1 and Novel 2 respectively. It can be observed that the aforementioned bead that develops as a result of the secondary velocities on the bottom of the jet enlarges as it moves closer to the bucket and some of this is disturbed during the bucket cut-in process, resulting in a non-optimal jet runner interaction for the Novel 2 case, where the bead is the largest.

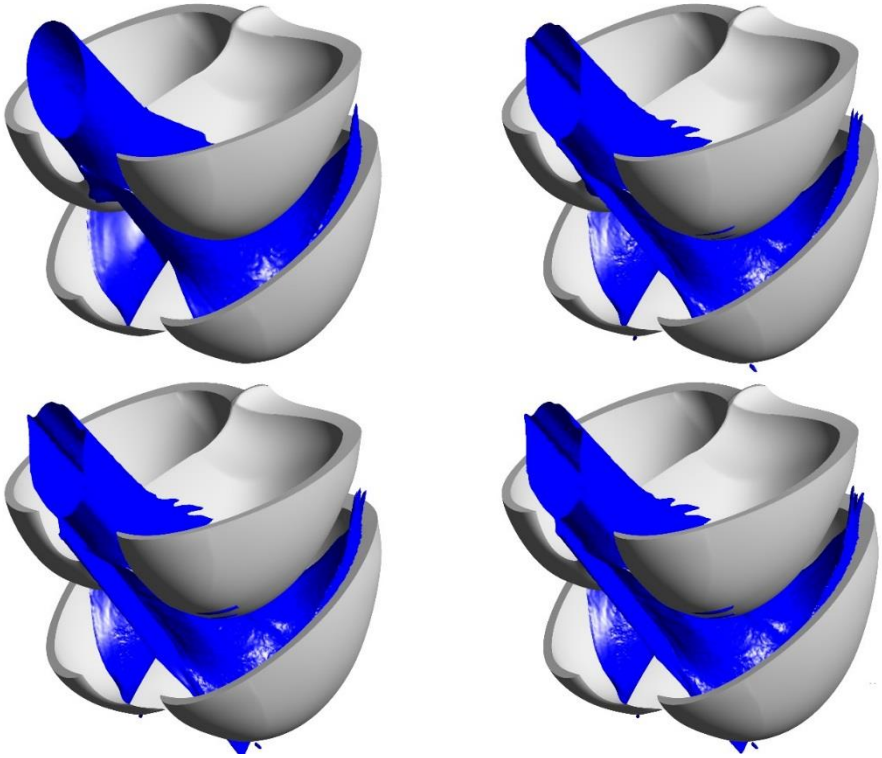

Figure 11. Volume Fraction (free-surface) Isosurface Plots for the 4 case studies.

4. Conclusions

This paper has investigated the influence of the nozzle and spear angle on the jet – runner interaction by considering four case studies. It has been demonstrated that a higher peak torque is experienced for the Novel cases with the highest peak torque on the inside of the bucket is experienced by the Novel 1 (110/70) design and consequently results in a higher efficiency. The reason for this is that while the jet velocity may not be as uniform as the Novel 2 case, a more compact jet with less surface disturbance ensures a more optimal exchange of kinetic energy with the runner.

One can conclude that the effect of friction is by far the largest contributor to hydraulic loss within the injector and as the area of the wetted surface of the spears in Novel 1 and 2 design is significantly less than the Standard design this results in a more uniform velocity distribution. Furthermore, the protrusion of the spear beyond the opening (to achieve the same flow) is larger for the Standard design, meaning a much more turbulent interchange between the free surface and spear immediately after exiting the nozzle, hence a delayed vena contracta in the Standard designs resulting in higher losses in the jet.

It should also be noted that with the steeper angled designs, there is an increased likelihood of jet breakup and droplet formation. These high velocity water droplets are known to cause damage to the runner and could become problematic for very high head applications. This has not been investigated at this stage but should be considered in future research.

In addition, these results go some way to demonstrate why experimentally (though not presented in this paper) there is a difference in efficiency between the upper and lower injector achieved with the three designs, with lower injector on the whole being slightly less efficient, but the Novel 2 case being the most efficient configuration – indicating that a combination of Novel 1 for upper injector and Novel 2 for lower injector could lead to an inherently higher overall efficiency for this turbine setup.

Acknowledgements
The authors would like to thank Gilbert Gilkes & Gordon Ltd, Lancaster University Renewable Energy and Fluid Machinery Group and the Laboratory of Hydraulic Turbomachines, NTUA.

References

[1] Nechleba M 1957 *Hydraulic Turbines: Their Design and Equipment* (Prague: Artia)

[2] Peron M, Parkinson E, Geppert L and Staubli T 2008 Importance of jet quality on Pelton efficiency and cavitation *Int. Conf. on Hydraulic Efficiency Measurements*

[3] Zeng C, Xiao Y, Lui Y, Zhang J, Wang Z, Fan H and Ahn S-H 2018 Hydraulic performance prediction of a prototype four-nozzle Pelton turbine by entire flow path simulation *Renewable Energy* **125** 270-82

[4] Staubli T, Abgottspon A, Weibel P, Bissel C, Parkinson E, Leduc J and Leboeuf F 2009 Jet quality and Pelton efficiency *Proc. of Hydro 2009*

[5] Židonis A and Aggidis G A 2015 State of the art in numerical modelling of Pelton turbines *Renewable and Sustainable Energy Reviews* **45** 135-44

[6] Benzon D, Židonis A, Panagiotopoulos A, Aggidis G A, Anagnostopoulos J S and Papantonis D E 2015 Impulse turbine injector design improvement using Computational Fluid Dynamics *ASME J. Fluids Eng.* **137**(4) 041106

[7] Benzon D, Židonis A, Panagiotopoulos A, Aggidis G A, Anagnostopoulos J S and Papantonis D E 2015 Numerical Investigation of the Spear Valve Configuration on the Performance of Pelton and Turgo Turbine Injectors and Runners *ASME J. Fluids Eng.* **137**(11) 111201

[8] Židonis A, Benzon D S, Panagiotopoulos A, Petley S, Aggidis G, Anagnostopoulos J and Papantonis D E 2017 Experimental investigation and analysis of the spear valve design on the performance of Pelton turbines: 3 case studies *Proc. of Hydro 2017*

[9] Santolin A, Cavazzini G, Ardizzon G and Pavesi G 2009 Numerical investigation of the interaction between jet and bucket in a Pelton turbine *Proc. IMechE Vol. 223 Part A: J. Power and Energy* **223** 721-8

[10] Chongji Z, Yexiang X, Wei X, Tao W, Jin Z and Zhengwei W 2016 Numerical Analysis of Pelton Nozzle Jet Flow Behavior Considering Elbow Pipe *IOP Conf. Ser.: Earth Environ. Sci.* **49** 022005

[11] Perrig A 2007 *Hydrodynamics of the Free Surface Flow in Pelton Turbine Buckets* PhD Thesis (Lausanne: EPFL)

[12] Parkinson E, Neury C, Garcin H, Vullioud C and Weiss T 2006 Unsteady analysis of a Pelton runner with flow and mechanical simulation *Int. Journal on Hydropower and Dams* **13**(2) 101-5